Chapter 1

Fermi Theory of Beta Decay

"Fermi's theory of β decay is the prototype of all weak-interaction calculations: a contact coupling times phase space."

standard nuclear-physics assessment [6, 14]

Lecture 18 introduced the continuous β spectrum and Fermi's golden rule. This lecture completes the original course derivation: plane-wave leptons and the allowed approximation, phase-space counting for electron and neutrino (with explicit volume cancellation), conversion to the electron kinetic energy K with the *correct* momentum–energy factor structure, the Coulomb Fermi function $F(Z, K)$, Fermi–Kurie plots, and the classification of allowed Fermi and Gamow–Teller transitions versus forbidden decays. The algebra follows Krane and Dunlap [6, 1, 14, 2].

1.1 Matrix element and plane-wave leptons

The partial decay rate depends on the matrix element of the weak interaction H_{int} between initial and final states:

$$|M_{if}|^2 = |\langle \psi_{\text{d}}\, \psi_e\, \psi_\nu | H_{\text{int}} | \psi_{\text{p}} \rangle|^2 \,. \tag{1.1}$$

For β^- decay, ψ_{p} is the parent nucleus, ψ_{d} the daughter, and ψ_e, ψ_ν the electron and antineutrino.

Free leptons are modelled as plane waves normalised in a large volume V:

$$\psi_e(\boldsymbol{r}) = \frac{1}{\sqrt{V}} e^{i\boldsymbol{p}_e \cdot \boldsymbol{r}/\hbar}, \qquad \psi_\nu(\boldsymbol{r}) = \frac{1}{\sqrt{V}} e^{i\boldsymbol{p}_\nu \cdot \boldsymbol{r}/\hbar}. \tag{1.2}$$

Expanding the electron factor,

$$\frac{1}{\sqrt{V}} e^{i\boldsymbol{p}_e \cdot \boldsymbol{r}/\hbar} = \frac{1}{\sqrt{V}} \left(1 + \frac{i\boldsymbol{p}_e \cdot \boldsymbol{r}}{\hbar} + \frac{(i\boldsymbol{p}_e \cdot \boldsymbol{r})^2}{2!\, \hbar^2} + \cdots \right). \tag{1.3}$$

The **allowed approximation** keeps only the leading constant term, equivalent to evaluating the lepton wave function at the origin ($\boldsymbol{r} = \boldsymbol{0}$). This corresponds to orbital angular momentum $\ell = 0$ for the lepton pair. The nuclear matrix element

$$M_{if} = \int \psi_{\text{d}}^*(\boldsymbol{r})\, H_{\text{int}}\, \psi_{\text{p}}(\boldsymbol{r})\, \mathrm{d}^3 r \tag{1.4}$$

is then nearly constant over the β spectrum, and the energy dependence comes from phase space [6, 1].

Squaring the transition amplitude, each lepton contributes a factor $1/V$:

$$|\langle\psi_f|H_{\text{int}}|\psi_i\rangle|^2 = \frac{|M_{if}|^2}{V^2}. \tag{1.5}$$

This $1/V^2$ will cancel against the V^2 from lepton phase space (Section 1.2).

1.2 Phase-space density and volume cancellation

1.2.1 Single-particle density of states

Consider a free particle of momentum p confined to a cube of side L, volume $V = L^3$. Standing-wave quantisation gives momentum components $p_x = n_x\pi\hbar/L$ with positive integers n_x. The spacing in each direction is $\pi\hbar/L$, so the volume per quantum state in momentum space is

$$\left(\frac{\pi\hbar}{L}\right)^3 = \left(\frac{h}{2L}\right)^3 = \frac{h^3}{8V}.$$

The factor 8 is essential: $h = 2\pi\hbar$.

The number of states with momentum magnitude between p and $p + \mathrm{d}p$ equals the number of lattice points in a spherical shell. Only the positive octant $(p_x, p_y, p_z > 0)$ contributes, giving shell volume $\pi p^2 \mathrm{d}p/2$. Dividing by the volume per state,

$$\mathrm{d}n = \frac{\pi p^2\,\mathrm{d}p/2}{h^3/(8V)} = \frac{4\pi p^2\,\mathrm{d}p\,V}{h^3}. \tag{1.6}$$

Equivalently, the uncertainty-principle argument assigns one state per cell

$$\Delta x\,\Delta y\,\Delta z\,\Delta p_x\,\Delta p_y\,\Delta p_z \sim h^3$$

in phase space, yielding the same result [6, 1].

1.2.2 Two leptons: product and cancellation

For β^- decay there are two free leptons. The combined number of final states in intervals $\mathrm{d}p_e$ and $\mathrm{d}p_\nu$ is the product:

$$\mathrm{d}n = \frac{4\pi p_e^2\,\mathrm{d}p_e\,V}{h^3}\cdot\frac{4\pi p_\nu^2\,\mathrm{d}p_\nu\,V}{h^3} = \frac{(4\pi)^2V^2}{h^6}\,p_e^2\,p_\nu^2\,\mathrm{d}p_e\,\mathrm{d}p_\nu. \tag{1.7}$$

From Fermi's golden rule (Lecture 18), the partial transition rate into this lepton momentum interval is

$$\mathrm{d}\lambda \propto \frac{|M_{if}|^2}{V^2}\cdot\frac{(4\pi)^2V^2}{h^6}\,p_e^2\,p_\nu^2\,\mathrm{d}p_e\,\mathrm{d}p_\nu = \frac{|M_{if}|^2}{h^6}\,p_e^2\,p_\nu^2\,\mathrm{d}p_e\,\mathrm{d}p_\nu. \tag{1.8}$$

The normalisation volume V cancels completely:

$$\frac{1}{V^2}\times V^2 = 1. \tag{1.9}$$

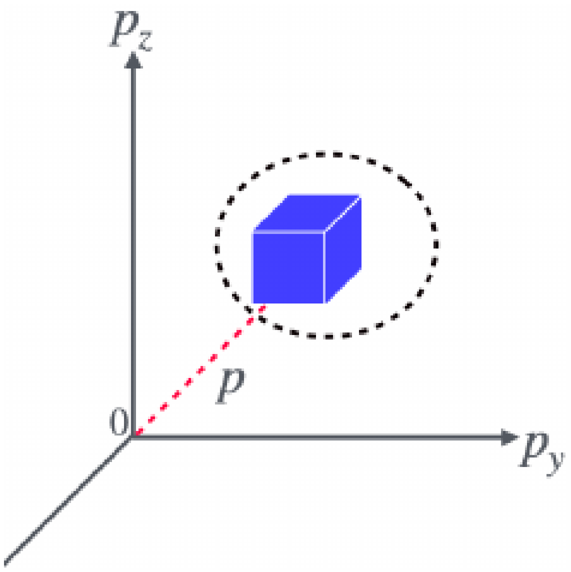

Figure 1.1: Momentum-space shell used to count lepton final states. Each quantum standing-wave state in the positive octant occupies $h^3/(8V)$ in momentum space; the factor 8 gives $\mathrm{d}n = 4\pi p^2\,\mathrm{d}p\,V/h^3$. Spin multiplicities, when summed explicitly, multiply this orbital count and may instead be absorbed into the overall weak-interaction constant.

The decay rate is independent of the arbitrary box size and depends only on $|M_{if}|^2$ and lepton momenta [6, 1, 14].

1.3 Spectrum in kinetic energy: correct momentum–energy factors

We now express $\mathrm{d}\lambda$ in terms of electron kinetic energy K.

Energy conservation. Neglecting nuclear recoil and neutrino mass,

$$Q = K + E_\nu, \qquad p_\nu c = E_\nu = Q - K, \qquad p_\nu^2 = \frac{(Q-K)^2}{c^2}. \tag{1.10}$$

Relativistic electron kinematics. Total electron energy $E_e = K + m_e c^2$. The invariant relation $E_e^2 = p_e^2 c^2 + m_e^2 c^4$ gives

$$(K + m_e c^2)^2 = p_e^2 c^2 + m_e^2 c^4, \tag{1.11}$$

so

$$p_e^2 = \frac{K^2 + 2K m_e c^2}{c^2} = \frac{K(K + 2m_e c^2)}{c^2}, \qquad p_e = \frac{\sqrt{K(K + 2m_e c^2)}}{c}. \tag{1.12}$$

Differentiating p_e with respect to K. From $p_e^2 c^2 = K^2 + 2K m_e c^2$, differentiate both sides:

$$2p_e c^2\,\mathrm{d}p_e = (2K + 2m_e c^2)\,\mathrm{d}K = 2(K + m_e c^2)\,\mathrm{d}K. \tag{1.13}$$

Hence

$$\mathrm{d}p_e = \frac{K + m_e c^2}{p_e c^2}\,\mathrm{d}K = \frac{K + m_e c^2}{\sqrt{K(K + 2m_e c^2)}}\,\frac{\mathrm{d}K}{c}. \tag{1.14}$$

Neutrino phase-space factor at fixed K. At fixed electron kinetic energy K, the final-state energy constraint fixes p_ν. For a massless neutrino, $\mathrm{d}E_\nu/\mathrm{d}p_\nu = c$, so integrating the energy-conserving delta function contributes $1/c$.

Assembling the spectrum. The differential rate in $\mathrm{d}K$ is proportional to $p_e^2\, p_\nu^2\, \mathrm{d}p_e/c$. Substituting (1.11), (1.10), and (1.14):

$$\begin{aligned}
\frac{p_e^2\, p_\nu^2}{c}\,\mathrm{d}p_e &\propto \frac{K(K + 2m_e c^2)}{c^2} \cdot \frac{(Q-K)^2}{c^2} \cdot \frac{K + m_e c^2}{\sqrt{K(K + 2m_e c^2)}}\,\frac{\mathrm{d}K}{c} \cdot \frac{1}{c} \\
&= \frac{(K + m_e c^2)\, K(K + 2m_e c^2)\,(Q-K)^2}{c^6\,\sqrt{K(K + 2m_e c^2)}}\,\mathrm{d}K \\
&= \frac{\sqrt{K(K + 2m_e c^2)}\,(K + m_e c^2)\,(Q-K)^2}{c^6}\,\mathrm{d}K.
\end{aligned} \tag{1.15}$$

Absorbing c^{-6} and other energy-independent constants into C, the **correct allowed spectrum** is

$$N(K)\,\mathrm{d}K = C\,|M_{if}|^2\,\underbrace{\sqrt{K(K + 2m_e c^2)}}_{p_e c}\,\underbrace{(K + m_e c^2)}_{E_e}\,(Q-K)^2\,\mathrm{d}K. \tag{1.16}$$

Key idea

Correct factor structure (memorise this form).

$$N(K)\,\mathrm{d}K \propto p_e\, E_e\, (Q-K)^2\,\mathrm{d}K, \tag{1.17}$$

$$N(K) \propto \sqrt{K(K + 2m_e c^2)}\,(K + m_e c^2)\,(Q-K)^2. \tag{1.18}$$

Here $p_e c = \sqrt{K(K + 2m_e c^2)}$ and $E_e = K + m_e c^2$. The factor $(Q-K)^2$ comes from the neutrino phase space. This is *not* the same as $K\sqrt{K + 2m_e c^2}\,(K + m_e c^2)(Q-K)^2$: the momentum factor is $p_e c = \sqrt{K(K + 2m_e c^2)}$, not $K\sqrt{K + 2m_e c^2}$. The erroneous extra factor $\sqrt{K}$ arises if one writes $p_e^2 \propto K(K + 2m_e c^2)$ but replaces $p_e\,\mathrm{d}p_e$ inconsistently [6, 1].

Dunlap's equation (9.27) writes the same result as $(T_e^2 + 2T_e m_e c^2)^{1/2}(Q - T_e)^2(T_e + m_e c^2)$, which is identical to (1.18) with $T_e = K$ [1, 6].

Momentum form. In terms of electron momentum p_e, with $K = (p_e c)^2/(2m_e c^2) = p_e^2/(2m_e)$ only in the *non-relativistic* limit and more generally from (1.12),

$$N(p_e)\,\mathrm{d}p_e \propto p_e^2\,(Q-K)^2\,\mathrm{d}p_e, \qquad K = K(p_e). \tag{1.19}$$

Both (1.17) and (1.18) must be used consistently when changing variables.

Non-relativistic and ultrarelativistic limits. For $K \ll m_e c^2$, $p_e c \simeq \sqrt{2m_e c^2 K}$ and $E_e \simeq m_e c^2$, so

$$N_{\mathrm{NR}}(K) \propto \sqrt{K}\,(Q-K)^2.$$

For $K \gg m_e c^2$, $p_e c \simeq E_e \simeq K$, so

$$N_{\mathrm{UR}}(K) \propto K^2(Q-K)^2.$$

These are limiting shapes, not interchangeable approximations; when $F(Z,K)$ is neglected they peak at $Q/5$ and $Q/2$, respectively.

1.4 Fermi function $F(Z,K)$

The plane-wave approximation ignores the Coulomb interaction between the emitted β particle and the daughter nucleus of charge $+Ze$. For β^- decay the interaction is attractive; for β^+ it is repulsive. Quantum mechanically, this modifies the electron/positron wave function near the nucleus and multiplies the spectrum by the **Fermi function**

$$F(Z,K) = \frac{2\pi\eta}{1-e^{-2\pi\eta}}, \tag{1.20}$$

with

$$\eta = \pm\frac{Ze^2}{4\pi\varepsilon_0\,\hbar v}. \tag{1.21}$$

The plus sign applies to β^- (electron attracted); the minus sign to β^+ (positron repelled). Here Z is the *daughter* atomic number and v is the lepton speed [6, 1].

Relativistic velocity. The relativistic relation is

$$v = \frac{p_e c^2}{E_e} = \frac{\sqrt{K(K+2m_e c^2)}}{K+m_e c^2}\,c. \tag{1.22}$$

A *non-relativistic* estimate $v \approx \sqrt{2K/m_e}$ is sometimes used for low K, but MeV-scale β particles require (1.22) [6, 1, 14].

Using $e^2/(4\pi\varepsilon_0) = \hbar c/137 \approx 1.44\,\mathrm{MeV\,fm}$ and $\hbar c \approx 197\,\mathrm{MeV\,fm}$,

$$\eta = \pm\frac{Z\times 1.44\,\mathrm{MeV\,fm}\,c}{197\,\mathrm{MeV\,fm}\,v} = \pm\frac{Z\times 1.44}{197}\,\frac{c}{v}. \tag{1.23}$$

The full spectrum including Coulomb corrections is

$$N(K)\,\mathrm{d}K \propto F(Z,K)\,\sqrt{K(K+2m_e c^2)}\,(K+m_e c^2)\,(Q-K)^2\,\mathrm{d}K. \tag{1.24}$$

$F>1$ enhances low-energy β^- electrons and suppresses low-energy positrons, explaining why the ^{64}Cu β^- and β^+ spectra in Lecture 18 differ in shape even though the bare phase space (1.16) is the same [1, 6].

Remark

The Fermi function (1.20) is most important at low K, where v is small and η is large. Its plane-wave limit is $F \to 1$ as $\eta \to 0$ (weak Coulomb field, $Z\alpha c/v \to 0$). Merely taking $K \to \infty$ gives $v \to c$ and $\eta \to \pm Z\alpha$, so F need not equal unity for a high-Z daughter. Fully relativistic Coulomb wave functions (Fermi–Longmire) are used in precision work [6, 1].

1.5 Fermi–Kurie plot

To test (1.24) against data, one linearises the spectrum. From (1.19) and (1.24), the momentum-space intensity is

$$I(p_e) \propto p_e^2\,(Q-K)^2\,F(Z,K). \tag{1.25}$$

Therefore

$$\sqrt{\frac{N(p_e)}{p_e^2\,F(Z,K)}} \propto (Q-K). \tag{1.26}$$

A plot of $\sqrt{N/(p^2F)}$ versus K (or total electron energy) is a **Fermi–Kurie plot**. For allowed transitions with constant $|M_{if}|^2$, the plot is a straight line intercepting $K = Q$ at zero intensity [6, 1].

^{66}Ga: a hindered Fermi caution, not a clean benchmark. $^{66}\mathrm{Ga}(0^+) \to {}^{66}\mathrm{Zn}(0^+) + \beta^+ + \nu_e$: $\Delta I = 0$ and no parity change permit an allowed Fermi transition, but the ground-state branch is strongly suppressed by isospin. Camp and Langer found $\log ft \simeq 7.9$ and reported an energy-dependent shape, making this branch sensitive to isospin mixing and higher-order terms. It must therefore not be presented as generic evidence that every allowed $0^+ \to 0^+$ Kurie plot is perfectly linear [31, 6].

^{91}Y: forbidden example. $^{91}\mathrm{Y}(\frac{1}{2}^-) \to {}^{91}\mathrm{Zr}(\frac{5}{2}^+) + e^- + \bar{\nu}_e$: $|\Delta I| = 2$ with parity change. The lepton pair must carry angular momentum; the $\ell = 0$ approximation fails. The Kurie plot (Fig. 1.3) bends upward (convex): a shape factor $S(K)$ multiplies the allowed spectrum [30, 6, 1].

1.6 Allowed Fermi and Gamow–Teller transitions

The lepton wave function expansion (1.2) links orbital angular momentum to the power of $\boldsymbol{p}\cdot\boldsymbol{r}/\hbar$. Keeping only the constant term is the *allowed* ($\ell = 0$) approximation.

Electron and neutrino each have spin $s = \frac{1}{2}$. The total leptonic spin can be

$$S = 0 \quad \text{(singlet, spins antiparallel)} \qquad \text{or} \qquad S = 1 \quad \text{(triplet, spins parallel)}. \tag{1.27}$$

With $\ell = 0$, the total leptonic angular momentum is $J = \ell + S = S$.

Fermi (vector) transitions. $S = 0$, $J = 0$. Selection rules:

$$\Delta I = 0, \qquad \Delta\pi = 0 \quad \text{(no parity change)}. \tag{1.28}$$

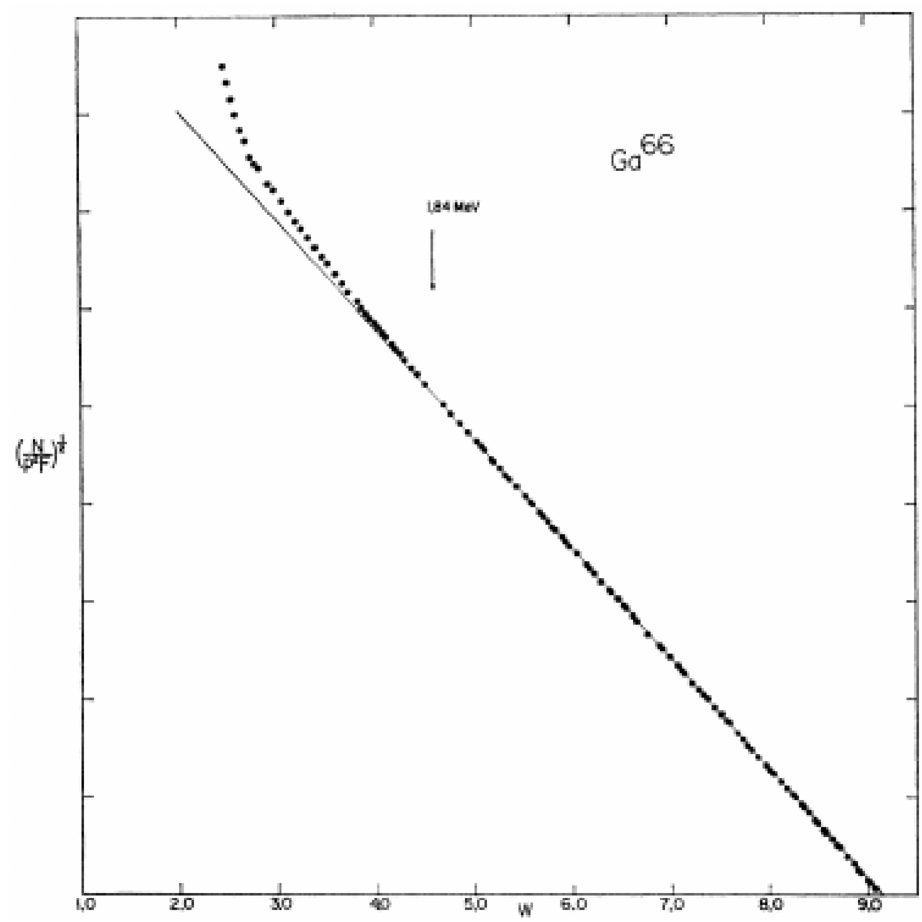

Figure 1.2: Fermi–Kurie plot for ^{66}Ga $\xrightarrow{\beta^+}$ ^{66}Zn, ground-state $0^+ \to 0^+$ branch. This branch is allowed by spin and parity but strongly isospin forbidden ($\log ft \simeq 7.9$); Camp and Langer reported a non-statistical shape. The restored original lecture panel reproduces the historical plot discussed by Camp and Langer [31]; see also [6, 1].

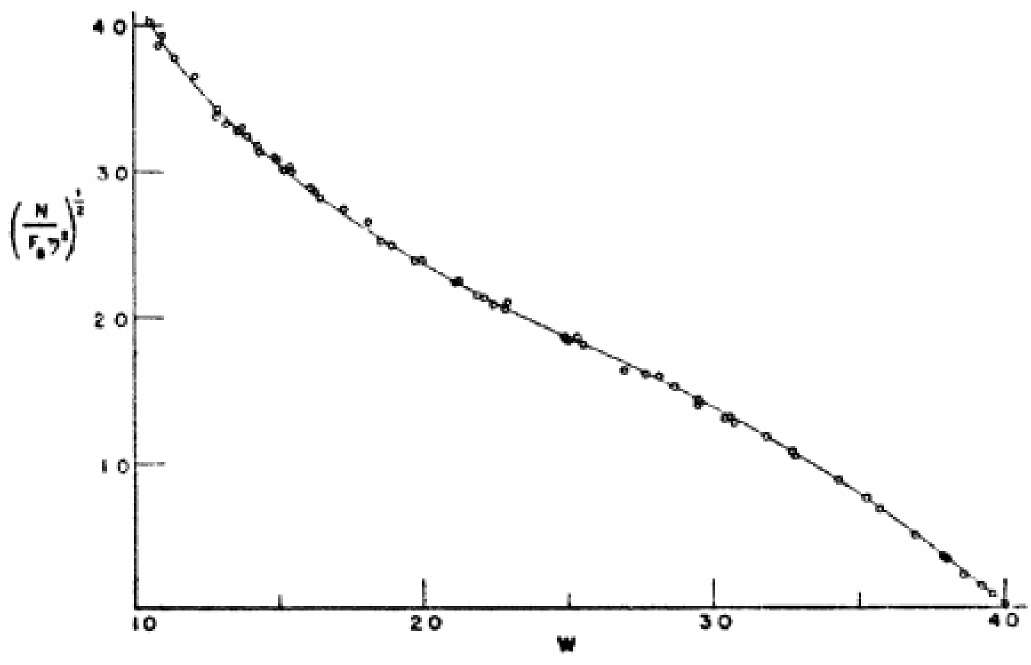

Figure 1.3: Fermi–Kurie plot for $^{91}\mathrm{Y} \xrightarrow{\beta^-} {}^{91}\mathrm{Zr}$: first-forbidden-unique transition. The conventional allowed reduction is curved, while division by the leading $p^2 + q^2$ shape factor restores a line. The restored original lecture panel reproduces the historical Langer–Price plot [30]; see also [6, 1] and `figures/lecture19/SOURCES.txt`.

Pure Fermi includes $0^+ \to 0^+$. In the allowed approximation the dimensionless nuclear matrix element is

$$M_F = \left\langle f \left| \sum_{k=1}^{A} \tau_k^{\pm} \right| i \right\rangle, \tag{1.29}$$

where $\tau_k^{\pm}$ converts a neutron to a proton or vice versa, according to the decay mode [6, 14].

Gamow–Teller (axial) transitions. $S = 1$, $J = 1$. Selection rules:

$$\Delta I = 0,\ \pm 1 \quad (\text{but not } 0^+ \to 0^+), \qquad \Delta\pi = 0. \tag{1.30}$$

The corresponding vector matrix element is

$$\boldsymbol{M}_{GT} = \left\langle f \left| \sum_{k=1}^{A} \boldsymbol{\sigma}_k \tau_k^{\pm} \right| i \right\rangle. \tag{1.31}$$

After the appropriate spin sums, an allowed mixed transition has nuclear strength

$$\mathcal{B}_{\text{allowed}} = g_V^2 |M_F|^2 + g_A^2 |M_{GT}|^2, \tag{1.32}$$

with vector and axial-vector couplings g_V and g_A. Their normalization must be stated consistently with the weak constant G_β; nuclear-medium calculations often use an effective g_A, so an extracted M_{GT} is convention dependent [6, 14, 2]. The pure Fermi limit has $M_{GT} = 0$; the pure Gamow–Teller limit has $M_F = 0$. For an unpolarized allowed rate the two contributions add as in (1.32), without an $M_F M_{GT}$ interference term.

Key idea

Allowed ($\ell = 0$): Fermi ($S = 0$, $\Delta I = 0$, no parity change) vs Gamow–Teller ($S = 1$, $\Delta I = 0, \pm 1$, not $0 \to 0$, no parity change). Both use the spectrum (1.18); the difference is in $|M_{if}|^2$, not in the leading phase space.

1.7 Forbidden transitions, shape factors, and ft values

If $\ell = 0$ transitions are suppressed by angular momentum or parity selection rules, the next term in the plane-wave expansion $(\boldsymbol{p} \cdot \boldsymbol{r}/\hbar)$ contributes. Transitions with leptonic orbital angular momentum $\ell \geq 1$ are called **forbidden**; the rate decreases rapidly as ℓ increases.

Order of forbiddenness. $\ell = 1$: first forbidden; $\ell = 2$: second forbidden; and so on [6, 1].

First-forbidden selection rules (summary). For $\ell = 1$, parity changes: $\Delta\pi = (-1)^{\ell} = -1$.

- First-forbidden Fermi ($\ell = 1$, $S = 0$): $\Delta I = 0, \pm 1$, $\Delta\pi = -1$.
- First-forbidden Gamow–Teller ($\ell = 1$, $S = 1$): $\Delta I = 0, \pm 1, \pm 2$, $\Delta\pi = -1$.

This orbital-and-spin coupling summary is only a mnemonic. Actual first-forbidden rates contain several vector and axial operators; "unique" transitions with $|\Delta I| = 2$ and parity change have a simpler leading shape factor, whereas non-unique transitions mix multiple matrix elements. The $^{91}\mathrm{Y}(\frac{1}{2}^-) \to {}^{91}\mathrm{Zr}(\frac{5}{2}^+)$ ground-state branch is first-forbidden unique [30, 6, 1].

Shape factor. Forbidden transitions multiply the allowed spectrum by an energy-dependent **shape factor** $S(K)$:

$$N(K)\,\mathrm{d}K = S(K)\,N_0(K)\,\mathrm{d}K, \tag{1.33}$$

where $N_0(K)\,\mathrm{d}K$ is the allowed form (1.24). When $S(K)$ is accounted for, the Kurie plot can be straightened [6, 1].

Dimensionless statistical rate function. Introduce electron total energy, momentum, and endpoint in electron-mass units:

$$W = \frac{E_e}{m_e c^2}, \qquad p = \frac{p_e c}{m_e c^2} = \sqrt{W^2 - 1}, \qquad W_0 = 1 + \frac{Q}{m_e c^2}.$$

For an allowed branch with a massless neutrino, the dimensionless integrated phase-space factor is

$$f(Z, W_0) = \int_1^{W_0} F(Z, W)\, pW\, (W_0 - W)^2\, \mathrm{d}W. \tag{1.34}$$

Finite-size, screening, radiative, recoil, and shape-factor corrections can be included in the integrand for precision work.

Partial half-life and the ft constant. With the coupling convention used in Eq. (1.32), the allowed partial rate is

$$\lambda_{\text{branch}} = \frac{G_\beta^2 m_e^5 c^4}{2\pi^3 \hbar^7} f(Z, W_0) \left[g_V^2 |M_F|^2 + g_A^2 |M_{GT}|^2 \right]. \tag{1.35}$$

If the branch fraction is b, its partial half-life is $t_{\text{branch}} = t_{1/2}^{\text{total}}/b$, not the total half-life. Since $\lambda_{\text{branch}} = \ln 2/t_{\text{branch}}$, rearrangement gives

$$f\, t_{\text{branch}} = \frac{K}{g_V^2 |M_F|^2 + g_A^2 |M_{GT}|^2}, \qquad K = \frac{2\pi^3 \hbar^7 \ln 2}{G_\beta^2 m_e^5 c^4} \simeq 6.1 \times 10^3\,\text{s}, \tag{1.36}$$

where the quoted numerical constant depends on whether g_V and CKM factors are included in G_β. Thus ft removes the leading phase-space dependence but still reflects the nuclear matrix elements and coupling convention. Values of $\log_{10}(ft/\text{s})$ classify transitions:

$\log_{10} ft$	Classification
3–3.5	Superallowed Fermi
~ 5	Allowed
6–10	First forbidden
> 10	Higher forbidden

Superallowed $0^+ \to 0^+$ Fermi decays determine the vector coupling G_V and, combined with muon decay, the CKM element V_{ud} [6, 1, 20].

Caution

"Forbidden" does not mean impossible: ^{91}Y β-decays with $t_{1/2} \approx 58\,\text{d}$. It means the transition is suppressed relative to allowed decays with similar Q [6].

Key idea

Students should remember:

- State counting: the positive-octant standing-wave cell is $h^3/(8V)$, hence $\mathrm{d}n = 4\pi p^2\,\mathrm{d}p\,V/h^3$; two leptons give $p_e^2 p_\nu^2$; V^2 cancels $1/V^2$ from $|M|^2$.
- Correct spectrum: $N(K) \propto p_e E_e (Q-K)^2$, equivalently $\sqrt{K(K+2m_e c^2)}(K+m_e c^2)(Q-K)^2$.
- Fermi function: $F = 2\pi\eta/(1-e^{-2\pi\eta})$, $\eta = \pm Ze^2/(4\pi\varepsilon_0 \hbar v)$, $v = p_e c^2/E_e$.
- Kurie plot: $\sqrt{N/(p^2 F)}$ vs K linear for allowed decays.
- Fermi: $S=0$, $\Delta I = 0$; GT: $S=1$, $\Delta I = 0, \pm 1$, not $0 \to 0$, with operators $\sum_k \tau_k^\pm$ and $\sum_k \boldsymbol{\sigma}_k \tau_k^\pm$. Forbidden transitions require operator-dependent shape factors.
- Comparative half-life: $f = \int_1^{W_0} F p W (W_0 - W)^2\,\mathrm{d}W$ and $ft_{\text{branch}} = K/(g_V^2|M_F|^2 + g_A^2|M_{GT}|^2)$.

1.8 Deeper physics: Fermi phase space and Kurie linearity

1.8.1 Allowed phase space in electron energy

For allowed β^- decay with $m_\nu = 0$, Fermi theory gives the partial spectrum (up to the Coulomb factor $F(Z,K)$)

$$\frac{\mathrm{d}N}{\mathrm{d}K} \propto |M_{if}|^2 \, F(Z,K) \, K \, (Q-K)^2 \, p_e, \tag{1.37}$$

where p_e is the electron momentum and $(Q-K)^2$ is the neutrino phase-space factor [6, 1]. The nuclear matrix element $|M_{if}|^2$ is nearly constant across the spectrum in the allowed approximation (lepton wave functions evaluated at the origin). All energy dependence then comes from lepton phase space and the Coulomb correction $F(Z,K)$, which enhances low-energy electrons in β^- decay of high-Z nuclei [6, 14].

Kurie plot for ^{64}Cu

Define the Kurie function $\sqrt{K(Q-K)^2 F(Z,K)^{-1}\, \mathrm{d}N/\mathrm{d}K}$. For an allowed transition with constant $|M_{if}|^2$, this quantity is linear in K and extrapolates to zero at $K = Q$ [6, 1]. Historical Kurie plots for ^{64}Cu show straight lines whose intercepts fix Q to better than 10 keV. Curvature signals forbidden transitions, neutrino mass, or incorrect $F(Z,K)$ [2].

1.8.2 The comparative half-life ft

Integrating (1.37) over K defines the phase-space factor $f(Z,Q)$. The product

$$ft = \frac{\ln 2}{f(Z,Q)\, |M_{if}|^2} \tag{1.38}$$

removes kinematics so that $\log_{10} ft$ reflects only the nuclear matrix element [6]. Superallowed $0^+ \to 0^+$ Fermi transitions cluster near $\log ft \approx 3.0$, setting the strength of the weak interaction. Forbidden decays have much larger $\log ft$ because additional lepton momentum factors suppress the rate [1, 14].

Key idea

Limits of the allowed approximation. The expansion of the electron plane wave at the origin fails when leptons carry orbital angular momentum ($\ell > 0$ for the lepton pair). Forbidden decays then acquire extra factors of K or $(Q-K)$ in the spectrum and curved Kurie plots. The allowed framework remains the baseline from which all higher-forbidden corrections are measured [6, 2].

1.8.3 Integrating the spectrum: the f factor

The total decay rate is obtained by integrating (1.37) from $K = 0$ to $K = Q$. The result defines the integrated phase-space factor $f(Z,Q)$, which depends on Z through $F(Z,K)$ and grows rapidly with Q. For superallowed $0^+ \to 0^+$ transitions, $\log ft \approx 3.0$; for first-forbidden decays, $\log ft$ can exceed 8 [6, 20]. The f-factor tabulations remove the kinematic Q dependence so that nuclear structure enters only through $|M_{if}|^2$. This separation is what allows measured half-lives from one isotope to calibrate weak-interaction strength for entirely different nuclei [1, 14].

1.8.4 Forbidden transitions and Kurie curvature

First-forbidden decays introduce additional lepton momentum factors (linear or quadratic in K) that curve the Kurie plot [6, 1]. The classification (allowed, first forbidden, second forbidden) is determined by nuclear spin and parity change together with the lepton orbital angular momentum required [14, 2]. Reactor antineutrino anomalies at short baseline have been discussed in terms of both sterile neutrinos and forbidden β branches of fission fragments; disentangling the two requires accurate shape factors [48]. The allowed Kurie linearity derived in this lecture is therefore not only a classroom exercise but a quality-control step in precision weak-interaction physics.

Comparative half-lives ft classify transitions: superallowed Fermi, allowed Gamow–Teller, and various forbidden degrees. When quoting $\log ft$, state whether screening and radiative corrections were applied. For double-β matrix elements, compare at least two many-body methods before converting a half-life limit into a mass limit.

1.9 Further physics from the literature

Neutrino mass and the endpoint. All expressions above assume $m_\nu = 0$, so $p_\nu c = E_\nu = Q - K$ and $(Q-K)^2$ appears in the spectrum. If $m_\nu \neq 0$, near the endpoint $(Q-K)$ is the neutrino total energy (neglecting recoil), and

$$p_\nu c = \sqrt{(Q-K)^2 - m_\nu^2 c^4}.$$

The massless factor $(Q-K)^2$ is therefore replaced by

$$(Q-K)\sqrt{(Q-K)^2 - m_\nu^2 c^4}\,\Theta(Q-K-m_\nu c^2).$$

The electron endpoint moves to $K_{\max} \simeq Q - m_\nu c^2 - E_{\rm rec}$, rather than remaining at Q. Precision β-spectroscopy near the tritium endpoint constrains m_{ν_e} [6, 14, 2].

Comparative half-lives and weak coupling. The product ft in (1.36) removes the calculated phase-space integral $f(Z,Q)$ so that $\log_{10} ft$ reflects only nuclear matrix elements. Superallowed $0^+ \to 0^+$ Fermi transitions (for example ^{14}O, ^{10}C) give the most precise value of G_V. Combined with muon decay, this determines the Cabibbo angle and V_{ud} in the quark mixing matrix [6, 1, 20].

From Fermi contact to W boson. Fermi's 1934 point interaction is the low-energy limit of charged-current exchange mediated by $W^\pm$ bosons ($m_W \approx 80\,\mathrm{GeV}/c^2$). At nuclear β energies the propagator momentum is so large that the interaction looks local, with strength set by G_F [14, 5, 2].

Experimental databases. Half-lives, Q-values, and branching ratios used in problems are tabulated in ENSDF and NuDat 3 [20, 21]. Kurie-plot data for ^{64}Cu, ^{66}Ga, and ^{91}Y appear in the classic papers by Langer *et al.* (1949) and Camp and Langer (1963), reproduced in Krane and Dunlap [6, 1].

From the literature

Basdevant *et al.* emphasise that the β spectrum is the earliest example of a three-body decay treated with relativistic phase space; the same methods reappear in muon and heavy-lepton decays [14]. Demtröder discusses modern tritium experiments and the KATRIN limit on m_{ν_e} [2].

Applications. The β spectrum shape enters dosimetry (medical isotopes), reactor antineutrino flux calculations, and detector calibration. NMR spin polarisation relies on β–γ angular correlations in allowed decays [13, 6].

1.9.1 Deriving Kurie linearity from phase space

For allowed β^- decay with constant $|M_{if}|^2$ and $m_\nu = 0$, divide (1.37) by $K(Q-K)^2F(Z,K)$ and take the square root:

$$\sqrt{\frac{\mathrm{d}N/\mathrm{d}K}{K(Q-K)^2F(Z,K)}} \propto |M_{if}|, \tag{1.39}$$

which is constant in K [6, 1]. Plotting the left-hand side versus K therefore gives a straight line intercepting $K = Q$. Curvature signals forbidden transitions (extra powers of K or $Q - K$), incorrect $F(Z,K)$, or neutrino mass near the endpoint [2]. This is why Kurie plots remain the standard diagnostic in precision β spectroscopy.

Superallowed $0^+ \to 0^+$ calibration

Superallowed Fermi transitions have $|M_{if}|^2 = T = 1$ isospin lowering with no angular-momentum barrier. Measured $\log ft$ values cluster near 3.0, fixing the vector coupling G_V [6, 20]. A 10% error in the integrated phase-space factor $f(Z,Q)$ propagates directly into G_V. Kurie-linearity checks on each transition verify that the allowed approximation holds before using the rate for fundamental-constant work [1, 14].

1.9.2 From $\log ft$ to γ selection rules and reactions

After β decay, daughter levels de-excite by γ emission governed by multipole selection rules (Lecture 20). A large $\log ft$ for the β branch implies a hindered weak matrix element; the subsequent γ cascade may include hindered $E1$ or $M1$ transitions with large internal conversion [6, 34]. In reactions, Gamow–Teller strength probed by charge-exchange experiments is the isospin analogue of allowed β decay (Lecture 21) [14, 51]. The phase-space factor f is the weak-interaction counterpart of the E_γ^{2L+1} phase space for photon emission.

Remark

Forbidden β decays feed reactor antineutrino systematics because their shape factors modify the spectrum at the few-percent level. Treating all fission fragments as allowed emitters biases oscillation fits. The Kurie formalism is the tool for separating those contributions [48, 6].

1.9.3 Charge-exchange reactions as β strength in reverse

Charge-exchange reactions such as (p, n) or $(^3\mathrm{He}, t)$ on stable targets populate the same Gamow–Teller strength that β decay would connect if isospin were reversed [14, 51]. The cross section at zero momentum transfer is proportional to $B(GT)$, the same reduced matrix element that sets $\log ft$ in β decay. This link explains why nuclear-structure calculations that quench $B(GT)$ in the shell model affect both reactor antineutrino fluxes and $0\nu\beta\beta$ matrix elements [50, 48]. Kurie linearity is the low-energy laboratory check that the phase-space factorisation is correct before importing $\log ft$ systematics into astrophysical networks.

1.9.4 Double beta decay and lepton-number violation

Two-neutrino double β decay ($2\nu\beta\beta$) is an allowed second-order weak process within the Standard Model; neutrinoless double β ($0\nu\beta\beta$) would prove that neutrinos are Majorana particles [6, 5, 49]. The phase-space treatment of Lecture 19 extends to $0\nu\beta\beta$ with a different lepton factor but the same nuclear matrix-element bottleneck [50, 48]. The $\log ft$ systematics for single β decay calibrate many-body methods that are then applied to $0\nu\beta\beta$ matrix elements. Ton-scale experiments searching for $0\nu\beta\beta$ are among the highest-priority construction projects in nuclear science [52, 49].

1.10 Deeper reading: phase space, ft values, and matrix elements

Fermi theory organises allowed spectra through phase space f and a nuclear matrix element. A linear Kurie plot is the signature of an allowed vector/axial transition with approximately constant $|M_{if}|^2$. Forbidden decays acquire shape factors; quenching of Gamow–Teller strength connects to Lecture 14 and to two-body currents.

Neutrinoless double-β decay reuses the same weak language at second order in lepton-number violation. Half-life limits translate into Majorana mass limits only after choosing a nuclear matrix element set: state that choice explicitly. Superallowed $0^+ \to 0^+$ Fermi decays remain the precision electroweak calibration points of nuclear β decay.

Vector versus axial probes

Pure Fermi transitions test the vector current and CKM unitarity inputs; Gamow–Teller transitions test axial strength and nuclear spin correlations. Mixing ratios in mixed transitions require correlation measurements. Keeping those channels distinct clarifies why quenching is primarily an axial-current story in medium-mass nuclei.

Phase-space sensitivity

Because f rises steeply with Q, a 50 keV mass error near a small endpoint strongly affects extracted $|M_{if}|^2$ from a measured half-life. Mass precision and β spectroscopy are coupled experimental programmes, not sequential afterthoughts.

Comparative half-life drill

Take a superallowed Fermi transition with known $t_{1/2}$ and Q, look up or approximate the phase-space factor f, and form ft. Compare with a free-neutron lifetime scale to see why nuclear matrix elements of order unity are special. Then take a strongly hindered forbidden decay and note the jump in $\log ft$.

Write a one-paragraph explanation of why $2\nu\beta\beta$ is allowed in the Standard Model while $0\nu\beta\beta$ is not, emphasising lepton number and the role of nuclear matrix elements in the rate. State that operator quenching lessons from Lectures 8 and 14 feed directly into those matrix elements. This paragraph is the conceptual endpoint of the weak-interaction arc that began with continuous spectra in Lecture 18.

Fermi theory converts Q values and matrix elements into rates. Comparative half-lives classify transitions; neutrinoless double-β decay reuses the same language at a deeper level.

In practice, rework one numerical estimate from the lecture with a different parameter set and compare the shift to the quoted experimental uncertainty. If the shift exceeds the uncertainty, the estimate is teaching a scale, not delivering a fit. That distinction keeps theoretical cartoons honest when they sit beside evaluated data tables and modern many-body calculations. Along the course arc, write one sentence linking this chapter backward and one forward: the discipline of those two sentences is as important as any single formula. Examination problems rarely ask for a literature review, but they do ask for the scale argument that literature reviews presuppose.

Synthesis problem

Write a half-page note that (i) restates the chapter's central scale or selection rule in one equation, (ii) evaluates it numerically for one concrete nucleus or energy, and (iii) names the neighbouring lecture that uses the result. Keep the note free of research-frontier speculation; the goal is fluency with the lecture physics itself. If an assumption fails (Born approximation, spherical mean field, allowed transition, one-dimensional barrier), state the failure mode in a final sentence. That habit converts passive reading into examination-ready understanding and makes the later research-frontier box read as an extension rather than a replacement.

Research frontier: Fermi theory, quenching, and $0\nu\beta\beta$

Fermi's golden-rule treatment (Lecture 19) still organises allowed spectra and ft values, but nuclear matrix elements for forbidden decays and for neutrinoless double-β decay require correlated many-body theory. Consistent two-body currents reduce GT quenching and revise $0\nu\beta\beta$ matrix-element estimates [50]. Ton-scale $0\nu\beta\beta$ experiments are a highest-priority construction recommendation of the 2023 nuclear-science long-range plan [52, 49, 48]. What remains uncertain is not whether lepton-number violation would be revolutionary if observed, but how large the nuclear matrix element is, and therefore how a half-life limit translates into a Majorana-mass limit. Forbidden β decays in nuclei relevant to reactor antineutrino spectra add a second applied frontier where shape factors and quenching must be controlled. The lecture's phase-space and selection-rule language remains the correct entry point to those advanced topics.

When comparing $0\nu\beta\beta$ half-life limits across isotopes, students should convert to an effective Majorana mass only after stating which matrix element set was assumed. Different many-body methods still disagree at the factor-of-two level in some cases, which dominates the particle-physics interpretation even when the experimental exposure is excellent.

Stating the matrix-element set used when converting a half-life limit into an effective Majorana mass is mandatory for an honest comparison across isotopes.

Student directions. (1) Derivation check: show why an allowed Kurie plot is linear for constant $|M_{if}|^2$. (2) Data estimate: extract $\log ft$ from a measured half-life and phase-space factor for one superallowed transition. (3) Short report: contrast $2\nu\beta\beta$ (Standard Model) with $0\nu\beta\beta$ (lepton-number violation) and the role of nuclear matrix elements.

1.11 Problems with solutions

Problem 19.1 — Derive the spectrum from phase space

Starting from $\mathrm{d}\lambda \propto p_e^2 p_\nu^2\, \mathrm{d}p_e/c$, where $1/c$ comes from the massless-neutrino energy delta function, with $p_\nu c = Q - K$ and relativistic electron kinematics, derive

$$N(K)\,\mathrm{d}K \propto \sqrt{K(K + 2m_e c^2)}\,(K + m_e c^2)\,(Q - K)^2\,\mathrm{d}K. \tag{1.40}$$

Show every algebraic step [1, 6].

Step-by-step

Step 1: Neutrino factor. $p_\nu c = E_\nu = Q - K$, so $p_\nu^2 = (Q - K)^2/c^2$.

Step 2: Electron momentum squared. From $E_e = K + m_e c^2$ and $E_e^2 = p_e^2 c^2 + m_e^2 c^4$:

$$p_e^2 c^2 = K^2 + 2K m_e c^2 \quad \Rightarrow \quad p_e^2 = \frac{K(K + 2m_e c^2)}{c^2}.$$

Step 3: Differentiate for $\mathrm{d}p_e$. From $p_e^2 c^2 = K^2 + 2K m_e c^2$:

$$2p_e c^2\,\mathrm{d}p_e = 2(K + m_e c^2)\,\mathrm{d}K \quad \Rightarrow \quad \mathrm{d}p_e = \frac{K + m_e c^2}{p_e c^2}\,\mathrm{d}K.$$

Step 4: Assemble.

$$\frac{p_e^2 p_\nu^2}{c}\,\mathrm{d}p_e = \frac{K(K + 2m_e c^2)}{c^2} \cdot \frac{(Q - K)^2}{c^2} \cdot \frac{K + m_e c^2}{p_e c^2}\,\mathrm{d}K \cdot \frac{1}{c}.$$

Step 5: Substitute p_e. Use $p_e = \sqrt{K(K + 2m_e c^2)}/c$:

$$\frac{p_e^2 p_\nu^2}{c}\,\mathrm{d}p_e = \frac{K(K + 2m_e c^2)(Q - K)^2(K + m_e c^2)}{c^6\sqrt{K(K + 2m_e c^2)}}\,\mathrm{d}K.$$

Step 6: Simplify. Cancel one factor $\sqrt{K(K + 2m_e c^2)}$ from numerator and denominator:

$$\frac{p_e^2 p_\nu^2}{c}\,\mathrm{d}p_e = \frac{\sqrt{K(K + 2m_e c^2)}\,(K + m_e c^2)\,(Q - K)^2}{c^6}\,\mathrm{d}K.$$

Step 7: Identify $p_e c$ and E_e.

$$\sqrt{K(K + 2m_e c^2)} = p_e c, \qquad K + m_e c^2 = E_e,$$

so $N(K)\,\mathrm{d}K \propto p_e E_e (Q - K)^2\,\mathrm{d}K$, as required [1, 6].

Problem 19.2 — Endpoint and maximum of $N(K)$

For allowed β^- decay with $Q = 1.0\,\mathrm{MeV}$ and $m_e c^2 = 0.511\,\mathrm{MeV}$, show that $N(K) = 0$ at $K = Q$ and estimate $K_{\max}$ where $N(K)$ peaks (numerically or graphically).

Step-by-step

At $K = Q$: the factor $(Q - K)^2 = 0$, so $N(Q) = 0$. This is the spectrum endpoint.
For the maximum, set $dN/dK = 0$ on the allowed form (ignoring F):

$$N(K) \propto \sqrt{K(K + 2m_e c^2)}\,(K + m_e c^2)\,(Q - K)^2.$$

It is convenient to differentiate $\ln N$:

$$\frac{K + m_e c^2}{K(K + 2m_e c^2)} + \frac{1}{K + m_e c^2} - \frac{2}{Q - K} = 0.$$

With $Q = 1.0\,\mathrm{MeV}$ and $m_e c^2 = 0.511\,\mathrm{MeV}$, the root is

$$K_{\mathrm{peak}} = 0.338\,\mathrm{MeV}.$$

This lies between the non-relativistic limiting estimate $Q/5$ and the ultrarelativistic estimate $Q/2$. The spectrum peaks well below Q because the $(Q - K)^2$ factor favors energy sharing with the neutrino [6, 1].

Problem 19.3 — Fermi parameter η

For β^- decay to a daughter with $Z = 30$, find η and comment on $F(Z, K)$ at $K = 0.10\,\mathrm{MeV}$ and $K = 1.0\,\mathrm{MeV}$. Use $v = p_e c^2/E_e$.

Step-by-step

At $K = 0.10\,\text{MeV}$:

$$p_e c = \sqrt{0.10 \times 1.122} = 0.335\,\text{MeV}, \quad E_e = 0.611\,\text{MeV},$$

$$v = \frac{p_e c^2}{E_e} = 0.548c, \qquad \eta = +\frac{30 \times 1.44}{197 \times 0.548} \approx 0.40.$$

Then $F = 2\pi\eta/(1 - e^{-2\pi\eta}) \approx 2.73$: Coulomb enhancement is large.
At $K = 1.0\,\text{MeV}$: $p_e c = \sqrt{1.0 \times 2.022} = 1.422\,\text{MeV}$, $E_e = 1.511\,\text{MeV}$, $v = 0.941c$, $\eta \approx 0.233$, and $F \approx 1.90$. Enhancement decreases at higher K [6, 1].

Problem 19.4 — Kurie plot intercept

A Fermi–Kurie plot of $\sqrt{N/(p^2F)}$ versus K for an allowed β^- decay is a straight line with slope $-0.50\,\text{MeV}^{-1}$ and intercept at $K = 2.50\,\text{MeV}$ on the horizontal axis. What is Q?

Step-by-step

For allowed decays, $\sqrt{N/(p^2F)} \propto (Q-K)$. The intercept where intensity vanishes is $K = Q$. Therefore $Q = 2.50\,\text{MeV}$ [6, 1].

Problem 19.5 — Classify ^{66}Ga and ^{91}Y

State whether each decay is allowed or forbidden, Fermi or Gamow–Teller, and predict the Kurie-plot shape.

Step-by-step

$^{66}\text{Ga}(0^+) \to {}^{66}\text{Zn}(0^+)$: $\Delta I = 0$, $\Delta\pi = 0$, so it is allowed Fermi by spin and parity. It is nevertheless strongly isospin forbidden ($\log ft \simeq 7.9$); the Camp–Langer spectrum was reported as non-statistical, so it is not a clean generic allowed benchmark [31, 6].
$^{91}\text{Y}(\frac{1}{2}^-) \to {}^{91}\text{Zr}(\frac{5}{2}^+)$: $|\Delta I| = 2$, parity changes: this is first-forbidden unique (minimum $\ell = 1$). The conventional allowed Kurie plot is non-linear until the first-forbidden-unique shape factor is included [30, 6, 1].

Problem 19.6 — Common error check

A student writes $N(K) \propto K\sqrt{K + 2m_ec^2}(K + m_ec^2)(Q - K)^2$. Explain why this differs from the correct formula and identify the extra factor.

Step-by-step

The correct momentum factor is $p_ec = \sqrt{K(K + 2m_ec^2)}$, not $K\sqrt{K + 2m_ec^2}$. The student expression has an extra factor of $\sqrt{K}$ relative to the correct form $\sqrt{K(K + 2m_ec^2)}(K + m_ec^2)(Q - K)^2$. This error typically arises from using $p_e^2 \propto K(K + 2m_ec^2)$ but failing to include the dp_e Jacobian correctly, or from confusing $p_e c$ with $K\sqrt{K + 2m_e c^2}$ [1, 6].

Bibliography

[1] R. A. Dunlap, *An Introduction to the Physics of Nuclei and Particles* (2nd ed.), IOP Publishing, Bristol (2023), DOI: 10.1088/978-0-7503-6094-4, Ch. 3 (Nuclear composition and size).

[2] W. Demtröder, *Nuclear and Particle Physics*, Undergraduate Lecture Notes in Physics, Springer, Cham (2023).

[3] S. Petrera, *Problems and Solutions in Nuclear and Particle Physics*, UNITEXT for Physics, Springer, Cham (2019).

[4] F. Terranova, *A Modern Primer in Particle and Nuclear Physics*, Oxford University Press (2021).

[5] S. D'Auria, *Introduction to Nuclear and Particle Physics*, Undergraduate Lecture Notes in Physics, Springer, Cham (2018).

[6] K. S. Krane, *Introductory Nuclear Physics*, Wiley, New York (1988).

[7] R. Hofstadter, "Electron scattering and nuclear structure," Rev. Mod. Phys. **28**, 214 (1956).

[8] H. F. Ehrenberg, R. Hofstadter, U. Meyer-Berkhout, D. G. Ravenhall, and S. E. Sobottka, "High-Energy Electron Scattering and the Charge Distribution of Carbon-12 and Oxygen-16," Phys. Rev. **113**, 666 (1959).

[9] H. Yukawa, "On the interaction of elementary particles. I," Proc. Phys.-Math. Soc. Japan **17**, 48 (1935).

[10] R. D. Woods and D. S. Saxon, "Diffuse surface optical model for nucleon-nuclei scattering," Phys. Rev. **95**, 577 (1954).

[11] H. G. J. Moseley, "The high-frequency spectra of the elements," Phil. Mag. **26**, 1024 (1913); **27**, 703 (1914).

[12] C. F. von Weizsäcker, "Zur Theorie der Kernmassen," Z. Phys. **96**, 431 (1935).

[13] P. Cappellaro, *Introduction to Applied Nuclear Physics* (MIT OpenCourseWare / LibreTexts), CC BY-NC-SA 4.0.

[14] J.-L. Basdevant, J. Rich, and M. Spiro, *Fundamentals in Nuclear Physics: From Nuclear Structure to Cosmology*, Springer, New York (2005).

[15] D. Tong, *Particle Physics*, Lecture notes (University of Cambridge / CERN school notes).

[16] M. G. Mayer, "On closed shells in nuclei. II," Phys. Rev. **75**, 1969 (1949).

[17] O. Haxel, J. H. D. Jensen, and H. E. Suess, "On the "magic numbers" in nuclear structure," Phys. Rev. **75**, 1766 (1949).

[18] T. Schmidt, "Über die magnetischen Momente der Atomkerne," Z. Phys. **106**, 358 (1937).

[19] L. W. Nordheim, "On spins, moments, and shells in nuclei," Phys. Rev. **78**, 294 (1950).

[20] Evaluated Nuclear Structure Data File (ENSDF), National Nuclear Data Center, Brookhaven National Laboratory, `https://www.nndc.bnl.gov/ensdf/`.

[21] NuDat 3, National Nuclear Data Center, Brookhaven National Laboratory, `https://www.nndc.bnl.gov/nudat3/`.

[22] N. J. Stone, "Table of nuclear magnetic dipole and electric quadrupole moments," At. Data Nucl. Data Tables **90**, 75 (2005); updated compilations at NNDC.

[23] W. N. Cottingham and D. A. Greenwood, *An Introduction to Nuclear Physics* (2nd ed.), Cambridge University Press, Cambridge (2001).

[24] H. Geiger and J. M. Nuttall, "The ranges of the α particles from the radioactive substances," Phil. Mag. **22**, 613 (1911).

[25] G. Gamow, "Zur Quantentheorie des Atomkernes," Z. Phys. **51**, 204 (1928).

[26] R. W. Gurney and E. U. Condon, "Wave mechanics and radioactive disintegration," Nature **122**, 439 (1928); Phys. Rev. **33**, 127 (1929).

[27] M. Wang, W. J. Huang, F. G. Kondev, G. Audi, and S. Naimi, "The AME 2020 atomic mass evaluation (II). Tables, graphs and references," Chin. Phys. C **45**, 030003 (2021).

[28] Laboratoire National Henri Becquerel (LNHB), Recommended decay data, `http://www.lnhb.fr/nuclear-data/nuclear-data-table/`.

[29] L. M. Langer, R. D. Moffat, and H. C. Price, Jr., "Low energy beta-ray spectra: P^{32} and Cu^{64}," Phys. Rev. **76**, 1725 (1949).

[30] L. M. Langer and H. C. Price, Jr., "Shapes of the beta-spectra of the forbidden transitions of Sb^{124}, Rb^{86}, Sr^{89}, Y^{91}, and Cs^{137}," Phys. Rev. **75**, 1769 (1949).

[31] D. C. Camp and L. M. Langer, "The shape of the ^{66}Ga positron spectrum and the contribution from $0^+ \to 0^+$ transitions," Phys. Rev. **129**, 1782 (1963).

[32] H. C. Verma, *Nuclear Physics: Fundamentals and Applications*, NPTEL/IIT Kanpur lecture series, `https://hcverma.in/ncl_phy_lectures`.

[33] International Atomic Energy Agency, *LiveChart of Nuclides*, evaluated structure, decay, reaction, and fission-yield data, `https://www-nds.iaea.org/relnsd/vcharthtml/VChartHTML.html`.

[34] T. Kibédi, T. W. Burrows, M. B. Trzhaskovskaya, P. M. Davidson, and C. W. Nestor, Jr., "Evaluation of theoretical conversion coefficients using BrIcc," Nucl. Instrum. Methods Phys. Res. A **589**, 202 (2008), DOI: 10.1016/j.nima.2008.02.051.

[35] D. A. Brown *et al.*, "ENDF/B-VIII.0: The 8th major release of the nuclear reaction data library with CIELO-project cross sections, new standards and thermal scattering data," Nucl. Data Sheets **148**, 1 (2018), DOI: 10.1016/j.nds.2018.02.001.

[36] B. Acharya *et al.*, "Solar fusion III: New data and theory for hydrogen-burning stars," Rev. Mod. Phys. **97**, 035002 (2025), DOI: 10.1103/8lm7-gs18.

[37] S. N. Ghoshal, "An experimental verification of the theory of compound nucleus," Phys. Rev. **80**, 939 (1950), DOI: 10.1103/PhysRev.80.939.

[38] D. Adhikari *et al.* (PREX Collaboration), "Accurate determination of the neutron skin thickness of ^{208}Pb through parity-violation in electron scattering," Phys. Rev. Lett. **126**, 172502 (2021), DOI: 10.1103/PhysRevLett.126.172502.

[39] B. T. Reed, F. J. Fattoyev, C. J. Horowitz, and J. Piekarewicz, "Implications of PREX-II on the equation of state of neutron-rich matter," Phys. Rev. Lett. **126**, 172503 (2021), DOI: 10.1103/PhysRevLett.126.172503.

[40] B. Hu *et al.*, "Ab initio predictions link the neutron skin of ^{208}Pb to nuclear forces," Nature Phys. **18**, 1196 (2022), DOI: 10.1038/s41567-022-01715-8.

[41] E. Epelbaum, H.-W. Hammer, and U.-G. Meißner, "Modern theory of nuclear forces," Rev. Mod. Phys. **81**, 1773 (2009), DOI: 10.1103/RevModPhys.81.1773.

[42] H.-W. Hammer, S. König, and U. van Kolck, "Nuclear effective field theory: Status and perspectives," Rev. Mod. Phys. **92**, 025004 (2020), DOI: 10.1103/RevModPhys.92.025004.

[43] T. Otsuka, A. Gade, O. Sorlin, T. Suzuki, and Y. Utsuno, "Evolution of shell structure in exotic nuclei," Rev. Mod. Phys. **92**, 015002 (2020), DOI: 10.1103/RevModPhys.92.015002.

[44] H. Hergert, S. K. Bogner, T. D. Morris, A. Schwenk, and K. Tsukiyama, "The in-medium similarity renormalization group: A novel ab initio method for nuclei," Phys. Rep. **621**, 165 (2016), DOI: 10.1016/j.physrep.2015.12.007.

[45] J. M. Lattimer and M. Prakash, "The equation of state of hot, dense matter and neutron stars," Phys. Rep. **621**, 127 (2016), DOI: 10.1016/j.physrep.2015.12.005.

[46] J. M. Lattimer, "Neutron stars and the nuclear matter equation of state," Annu. Rev. Nucl. Part. Sci. **71**, 433 (2021), DOI: 10.1146/annurev-nucl-102419-124827.

[47] B. P. Abbott *et al.* (LIGO Scientific Collaboration and Virgo Collaboration), "GW170817: Observation of gravitational waves from a binary neutron star inspiral," Phys. Rev. Lett. **119**, 161101 (2017), DOI: 10.1103/PhysRevLett.119.161101.

[48] M. J. Dolinski, A. W. P. Poon, and W. Rodejohann, "Neutrinoless double-beta decay: Status and prospects," Annu. Rev. Nucl. Part. Sci. **69**, 219 (2019), DOI: 10.1146/annurev-nucl-101918-023407.

[49] M. Agostini, G. Benato, J. A. Detwiler, J. Menéndez, and F. Vissani, "Toward the discovery of matter creation with neutrinoless $\beta\beta$ decay," Rev. Mod. Phys. **95**, 025002 (2023), DOI: 10.1103/RevModPhys.95.025002.

[50] P. Gysbers *et al.*, "Discrepancy between experimental and theoretical β-decay rates resolved from first principles," Nature Phys. **15**, 428 (2019), DOI: 10.1038/s41567-019-0450-7.

[51] H. L. Crawford, K. Fossez, S. König, and A. Spyrou, "A vision for the science of rare isotopes," Annu. Rev. Nucl. Part. Sci. **74**, 141 (2024), DOI: 10.1146/annurev-nucl-121423-091501.

[52] Nuclear Science Advisory Committee, *A New Era of Discovery: The 2023 Long Range Plan for Nuclear Science*, U.S. Department of Energy and National Science Foundation (2023), `https://nuclearsciencefuture.org/`.

[53] S. A. Giuliani, Z. Matheson, W. Nazarewicz, E. Olsen, P.-G. Reinhard, J. Sadhukhan, B. Schuetrumpf, N. Schunck, and P. Schwerdtfeger, "Colloquium: Superheavy elements: Oganesson and beyond," Rev. Mod. Phys. **91**, 011001 (2019), DOI: 10.1103/RevModPhys.91.011001.

[54] N. Schunck and D. Regnier, "Theory of nuclear fission," Prog. Part. Nucl. Phys. **125**, 103963 (2022), DOI: 10.1016/j.ppnp.2022.103963.

[55] I. Counts, J. Hur, D. P. L. Aude Craik, H. Jeon, C. Leung, J. C. Berengut, A. Geddes, A. Kawasaki, W. Jhe, and V. Vuletić, "Evidence for nonlinear isotope shift in Yb^+ search for new boson," Phys. Rev. Lett. **125**, 123002 (2020), DOI: 10.1103/PhysRevLett.125.123002.

[56] I. Angeli and K. P. Marinova, "Table of experimental nuclear ground state charge radii: An update," At. Data Nucl. Data Tables **99**, 69 (2013), DOI: 10.1016/j.adt.2011.12.006.

[57] S. Kraemer *et al.*, "Observation of the radiative decay of the ^{229}Th nuclear clock isomer," Nature **617**, 706 (2023), DOI: 10.1038/s41586-023-05894-z.